



Detecting, Distinguishing, and Counting Protein Aggregates using Total Holographic Characterization®

Introduction

Protein aggregation is a major challenge in the biopharmaceutical industry [1-6]. The FDA has highlighted the dangers of an immunogenic response elicited by the presence of protein aggregates in protein-based pharmaceutical formulations [7]. Accurately detecting protein aggregate concentrations and understanding their mechanisms of formation are crucial to ensuring maximum drug efficacy and safety, especially in the critical size range of 200nm to 2 μm [8-11]. In addition to detecting protein aggregates, other common contaminants are silicone oil, air bubbles, metal particles and degradation products of surfactants or other excipients in biologic formulations [12-15]. To distinguish protein aggregates from other contaminants, particle composition must be determined. Few technologies currently exist that can accurately count and simultaneously identify the composition of sub-visible particles in suspension.

Here we describe Total Holographic Characterization® (THC), a revolutionary technology that can detect, distinguish and count protein aggregates [16-18]. THC is an efficient optical approach that offers accurate, quantitative information about individual particles as well as a statistical overview of sample properties. An essential advantage of THC is the ability to detect particle refractive index in addition to particle size. Refractive index is used to identify particle composition, to distinguish particles of different materials even when they are the same size. Figure 1, shown below, illustrates the unique strength of this

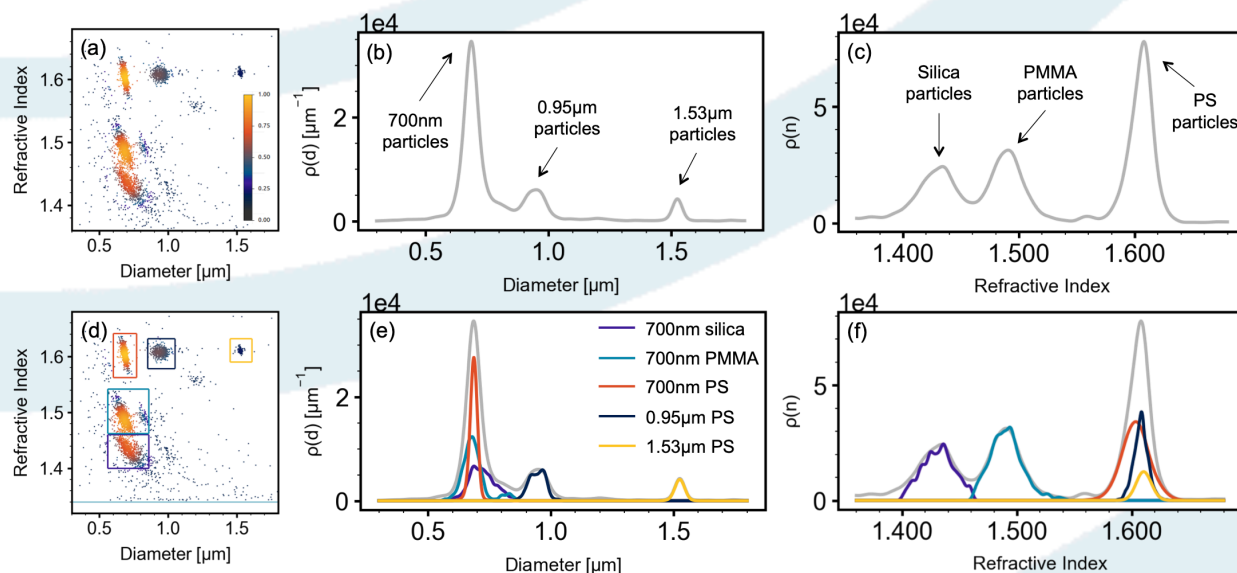


Figure 1: Results of THC analysis of a sample containing the following microspheres: 700nm silica, 700nm PMMA, 700nm PS, 0.95μm PS, and 1.53μm PS. (a) Scatter plot of particle diameter (horizontal axis) and refractive index (vertical axis). Color represents the density of points in the region, where warmer colors (yellow) represent higher density regions and cooler colors (blue) represent lower density regions. (b) Size density distribution of the same sample. The area under the curve represents the number of particles in that region of the curve. Peaks represent the most common particle sizes. (c) Refractive index density distribution of the same sample. The area under the curve represents the number of particles in that region of the curve. Peaks represent the most common particle refractive indexes. (d) The same scatter plot as in (a) with different particle populations delineated by colored boxes. (e) The same size density curve as in (b), with the size density curves of each particle population included in their respective colors based on how they were delineated in (d). (f) The same refractive index density curve as in (c), but with the size density curves of each particle population included in their respective colors based on how they were delineated in (d).



technology. Figure 1a shows a composite sample analyzed with xSight, Spheryx's implementation of THC. This sample is composed of a mix of 5 different microsphere species of three different sizes and made of three different materials. Figure 1a is a scatter plot with diameter plotted on the horizontal axis and the refractive index on the vertical axis. Each point on the plot represents a single particle detected by xSight. The color of each point represents the density of points in the region, where warmer colors (yellow) represent higher density regions and cooler colors (blue) represent lower density regions as indicated by the color bar in the bottom right section of Figure 1a. On this plot, five clusters of points can be identified: three are at a particle diameter of 700nm, one at 0.95 μ m, and one at 1.53 μ m. These clusters of points correspond to the 5 different species present in this sample and are delineated by user-defined colored boxes shown in Figure 1d.

Figure 1b shows a size density distribution of the same data set. The area under the curve for a given size range represents the number of particles in that size range. The peaks show the most common sizes of particles in this sample. The tallest peak in this curve is at 700nm since the most common particle size in this sample is 700nm. The two other peaks represent the 0.95 μ m particles and the 1.53 μ m particles. This type of curve is what most other particle characterization technologies would produce for this sample. While size is accurately determined, it is impossible to identify how many particle species are present. From this curve alone, it would be easy to conclude, erroneously, that this sample contains only three particle species, while in reality it contains five. The presence of 5 species is made clear by distinguishing clusters of points based on their refractive index, as seen in Figure 1d. Figure 1e shows the same density curve as in Figure 1b, but also adds the density curves of each particle species according to the colors of the user-defined regions in Figure 1d. In Figure 1e, the tallest peak can be separated into 3 peaks representing 3 different species of 700nm particles (represented by orange, cyan, and violet curves). The 3 different 700nm particle types are polystyrene (PS), PMMA, and silica. The refractive index of each particle type, automatically measured with THC, identifies the composition. Figure 1c shows the refractive index density distributions. The 3 peaks in this plot show that there are particles of 3 different compositions in this sample, at refractive indexes of 1.43, 1.49, and 1.61. These refractive indexes correspond to silica, PMMA, and PS respectively. The PS peak is the tallest because there are more PS spheres in this sample than of any other material. Figure 1f shows the same refractive index curve as Figure 1c with the five species of particles identified by their respective colors. The PS curve can be separated into three types of PS microspheres in this sample: 700nm in diameter, 0.95 μ m in diameter, and 1.53 μ m in diameter.

In the same way that xSight can distinguish PS, PMMA and silica particles, it can also distinguish protein aggregates from other common contaminants such as silicone oil and breakdown products of surfactants. Measurements of model samples of proteins are presented below to demonstrate these capabilities.

Methods

All samples shown in this note were measured with xSight. To use xSight, 30 μ L of the sample are placed in xCell, Spheryx's microfluidic sample chip, and the start button is pressed to begin the measurement. xSight automatically flows the sample through a microfluidic channel in xCell, illuminates the sample with a laser, records particle holograms, and begins analysis. The sample never leaves xCell, eliminating the need for cleaning and any danger of cross-contamination. Depending on the concentration of particles and the user-selected volume to be analyzed, the analysis can take between 10 and 40 minutes. Users select a volume between 0.2 μ L to 5 μ L. As data is analyzed results are plotted on the screen in real time. During analysis, particles are counted in a precisely measured volume to yield accurate concentrations. In addition to particle count and concentration, xSight reports the size, refractive index and the morphology of the detected particles.

Preparation of samples presented in this note, such as IgG protein aggregates and other contaminants, are detailed in several publications [16-18] and are briefly outlined here:

- Solutions of IgG were prepared by dissolving human IgG in filtered deionized water at room temperature to a concentration of 1 mg/mL. Protein aggregates formed spontaneously at room temperature.
- Silicone oil emulsions were prepared by adding silicone oil to deionized water and shaking the sample

vigorously by hand.

- Oleic acid samples were created by dissolving oleic acid in methanol at 20% followed by a 10-fold dilution in deionized water.
- Air bubble samples were created by rapidly ejecting an aqueous solution of polysorbate 20 (1mg/mL) and sucrose (64% by weight) from a syringe.

Results

Distinguishing protein aggregates from silicone oil

To accurately measure the concentration of protein aggregates in a formulation, it is essential to distinguish them from other contaminants. Silicone oil is often found in biological formulations as it easily elutes from the surfaces of syringes, plastic tubes and other medical or lab equipment, and can be difficult to distinguish from protein aggregates. By identifying particle composition, xSight can distinguish particles of different species even when they are the same size. Figure 2 below shows a mix of silicone oil and IgG protein aggregates in water. As in Figure 1a, Figure 2a is a scatter plot, where each point on the plot represents a single particle detected with xSight. The color of each point represents the density of points in the region, where warmer colors (yellow) represent higher density regions and cooler colors (blue) represent lower density regions as indicated by the color bar in the top right section of Figure 2a.

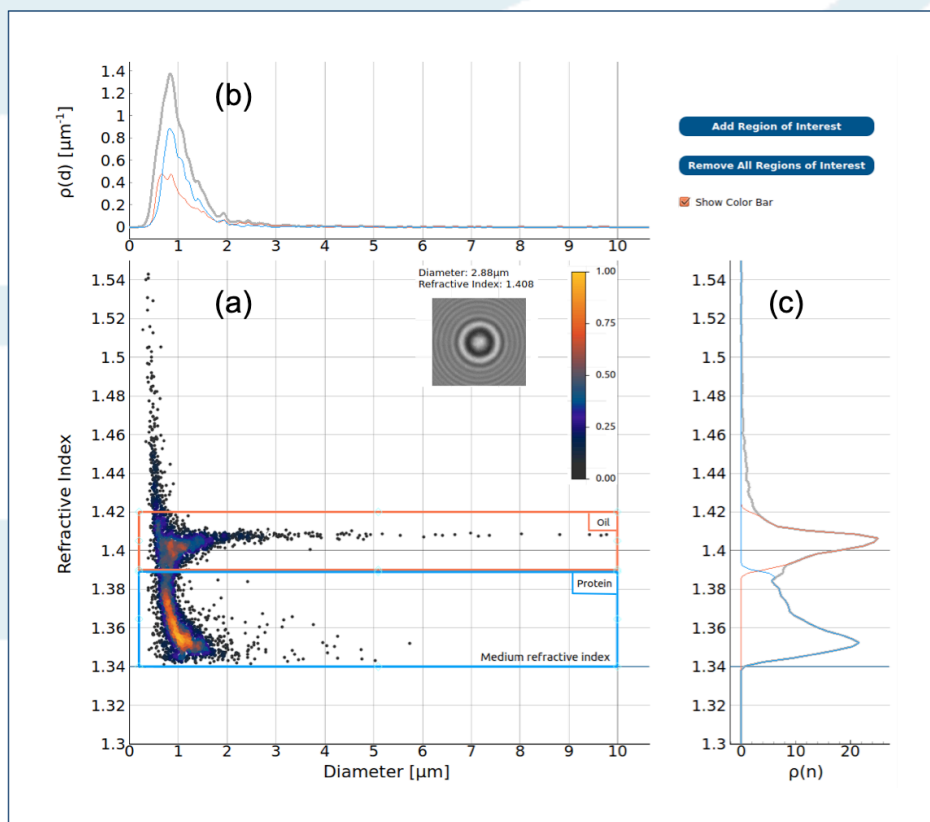


Figure 2: (a) Scatter plot of size vs. refractive index of particles detected in a sample of silicone oil and IgG aggregates. This figure is taken from xSight software displays. Each point represents the measurement of a single particle. The coloring is based on the density of points with yellow representing highest density and gray representing lowest density regions. The inset image is the hologram of a single silicone oil droplet of 2.88 μm diameter and a refractive index of 1.408 (b) Size density curves: the orange curve corresponding to data in the orange box identifying silicone oil droplets, the cyan curve corresponding to data in the cyan box identifying protein aggregate particles, and the gray curve represents all data. (c) Refractive index density curves with the same coloring as (b).

Particle refractive index is shown on the vertical axis and particle diameter is on the horizontal axis. Particles with a refractive index near 1.41 are identified as oil droplets corresponding to the refractive index of silicone oil (1.41). Particles at lower refractive indexes, between 1.34 and 1.39, are identified as protein aggregates. The orange and cyan boxes are user-defined regions of interest meant to delineate different species of particles within one sample. In this case the orange box contains oil droplets and the cyan box contains



protein aggregates. The data shown here represents characterization of 3995 particles detected in 3 μL of this sample, 1553 of which are identified as silicone oil and 2159 are IgG aggregates. The user is able to click on any of the points to see a representative hologram for that particle. A representative hologram of one of the particles in this distribution is shown as an inset in Figure 2a.

Silicone oil and protein aggregates have different refractive indexes and are easily distinguishable by xSight. In Figure 2a one can see how distinct the two species are based on how neatly they fall into the two regions of interest (the orange and the cyan boxes). Also evident is how distinguishable they are based on the density distributions shown in Figure 2c. The curves in Figure 2b represent the probabilities of finding a particle of a given species at a particular size. The orange curve represents points outlined by the orange box, the cyan curve represents points outlined by the cyan box and the gray curve represents all of the points. The curves in Figure 2c similarly represent density distributions but for refractive index instead of particle size. The overlap of the orange and the cyan curves in Figure 2b shows that silicone oil droplets and protein aggregates have similar sizes. Their similar size distributions make them difficult to distinguish with other particle characterization technologies. A unique benefit of THC is the ability to determine particle refractive index in addition to size. From the refractive index density distribution shown in Figure 2c, the orange curve and the cyan curve are distinct and well-separated, which shows the ability to distinguish the two particle species in this sample, based on an objective measurement of a physical characteristic of the particle.

In addition to measuring particles' size and refractive index, Spheryx's software also determines particle concentrations as shown in Figure 3. As in Figure 2, the orange curve represents particles identified as silicone oil, the cyan curve represents particles identified as protein aggregates, and the dark blue curve represents all detected particles. The bottom of Figure 3 shows a cumulative concentration table. The concentration data for each species is tabulated according particle size in $1\mu\text{m}$ bins.

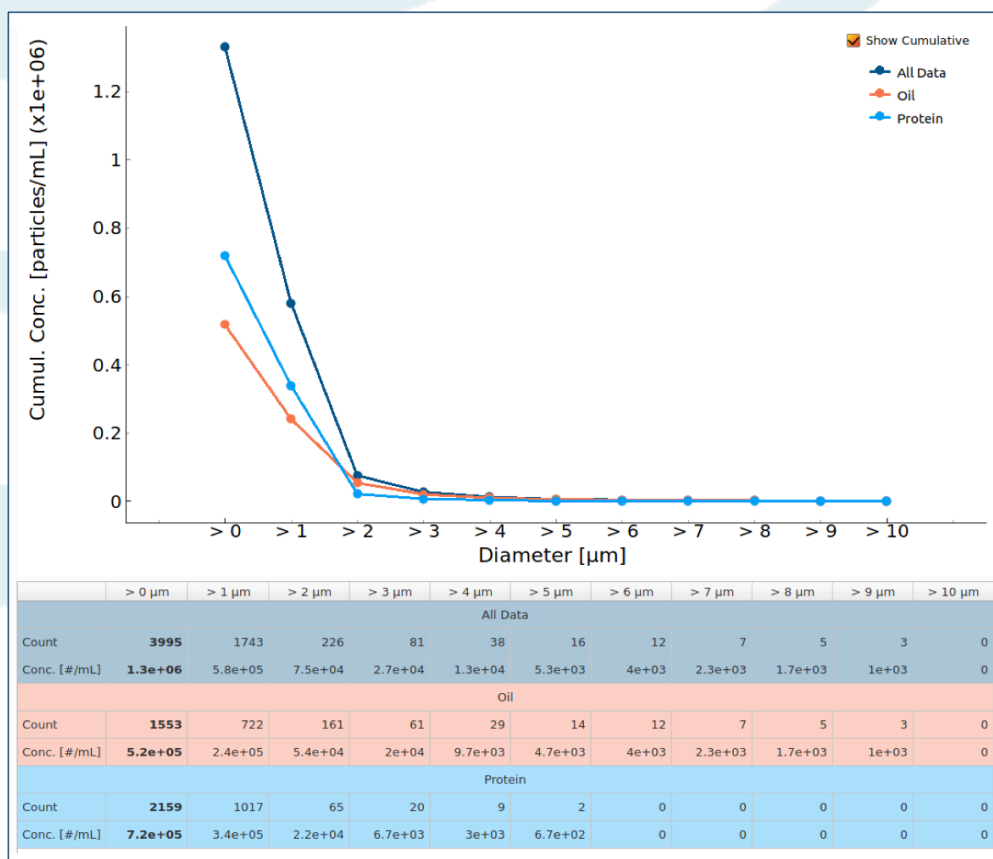


Figure 3: This plot and data table is taken from xSight software display. The top graph shows a plot of cumulative particle concentrations as a function of particle size. The orange curve corresponds to particles identified as silicone oil in Figure 2, the cyan curve corresponds to particles identified as protein aggregates in Figure 2 and the dark blue curve corresponds to all particles. The table breaks down particle concentrations by size into $1\mu\text{m}$ bins. Orange rows correspond to silicone oil, cyan rows correspond to protein aggregates and dark blue rows correspond to all particles. In this tab, the user chooses to view cumulative or non-cumulative concentrations.

Identifying and distinguishing surfactant degradation among other contaminants in protein formulations

The use of surfactants is common in biopharmaceutical formulations. Surfactant breakdown products can be difficult to distinguish from protein aggregates. One common breakdown product of polysorbate 20 is oleic acid. In Figure 4 below we demonstrate the ability to identify and quantify the presence of oleic acid in a mixture of protein aggregates and silicone oil.

Figure 4 represents data from 4875 particles in a 5 μ L sample consisting of a mixture of silicone oil droplets, protein aggregates and oleic acid droplets in water. Figure 4a shows a scatter plot of particle size plotted against particle refractive index as in Figure 2a. Unlike in Figure 2a, here three distinct particle species are easily identified. The population at the highest refractive index, centered at around 1.48, is identified as oleic acid and is outlined with a violet box. As in Figure 2a, the population centered at around 1.41 is a silicone oil emulsion (orange box) and the population at the lowest refractive index, between 1.34 and 1.39, is IgG aggregates (cyan box). Since particles of all three species have similar sizes, the size distribution densities in Figure 4b overlap. This shows how unfeasible it is to distinguish these contaminants solely based on particle size. In particular, based on size alone, it would be nearly impossible to detect the presence of oleic acid in this sample. By measuring the refractive index, the three species are distinguishable as evidenced by the separation of the colored boxed in Figure 4a and the three well-separated peaks in the refractive index density curves in Figure 4c.

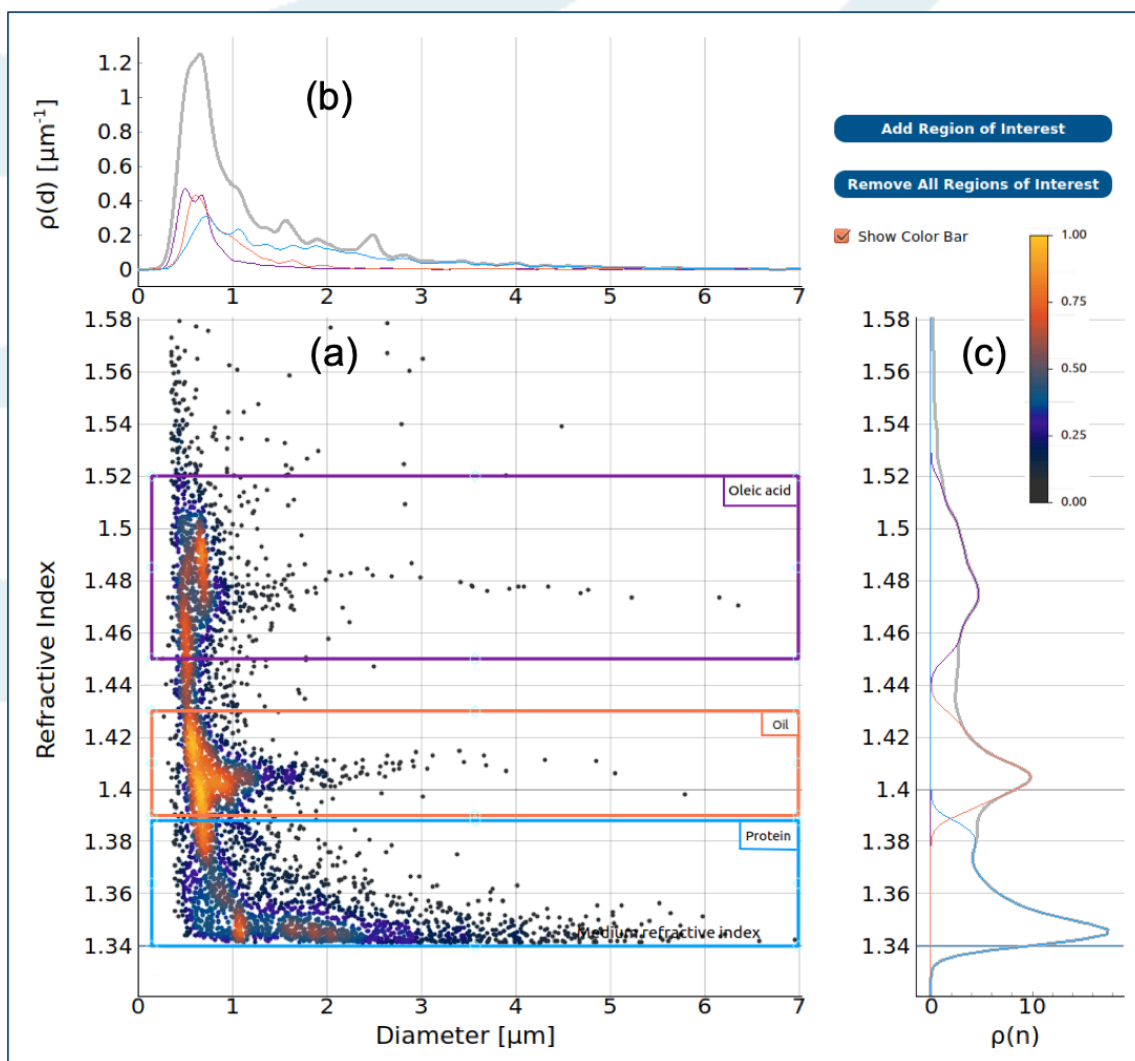


Figure 4: Scatter plot and probability density distributions for a sample of silicone oil, IgG aggregates and oleic acid.

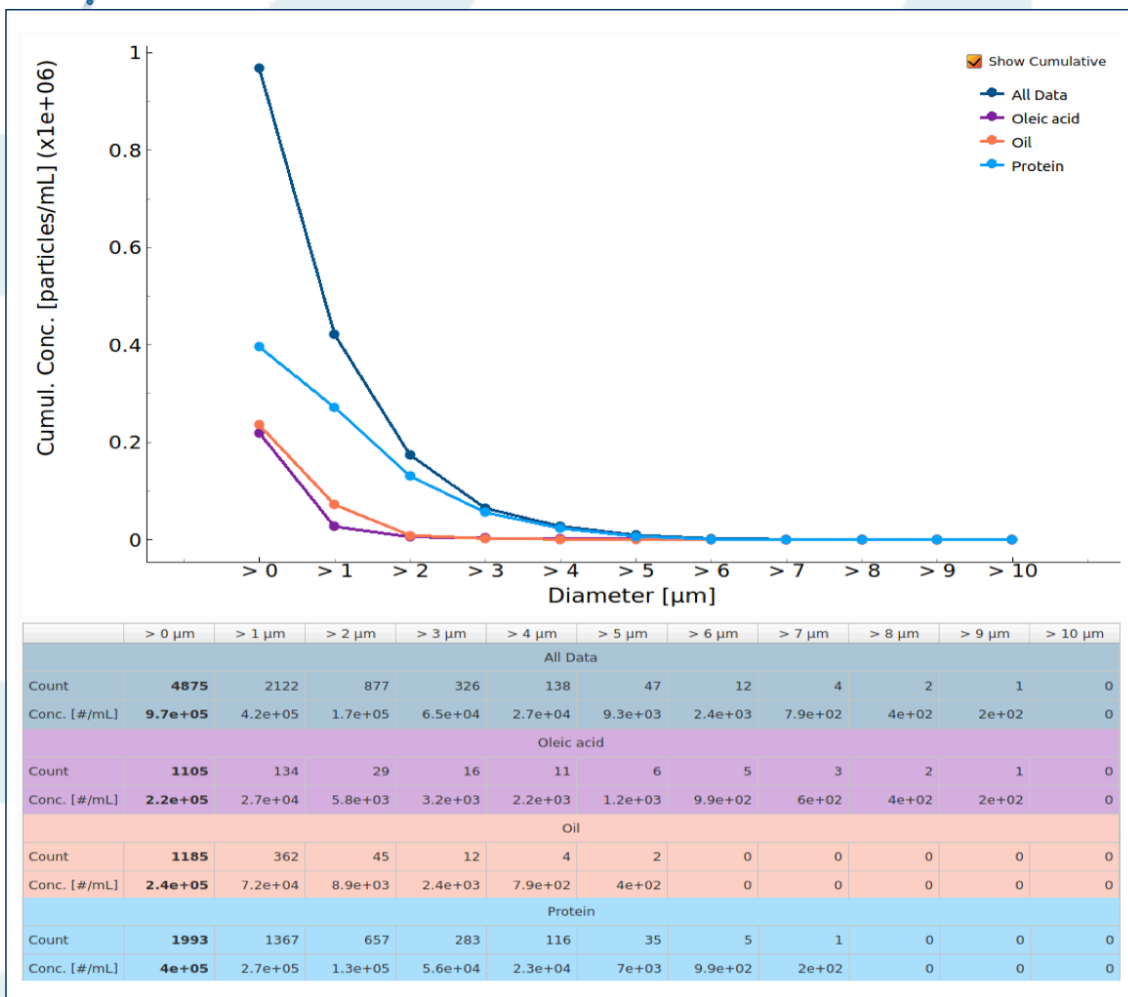


Figure 5: Cumulative concentrations curves as a function of particle size and a table as in Figure 4 but for a sample of silicone oil, IgG aggregates and oleic acid.

In addition to detecting surfactant breakdown products like oleic acid, xSight determines accurate concentrations of each contaminant simultaneously in a single measurement. Figure 5 shows a graph and a table of cumulative concentrations of the three species shown in Figure 4. The table in Figure 5 breaks down the concentration of three species by size in 1µm bins.

Detecting air bubbles and distinguishing them from silicone oil

Another common contaminant in protein formulations is air bubbles. Air bubbles often form in viscous samples that undergo fast ejection and aggressive agitation [19, 20]. Air bubbles can be notoriously difficult to identify, but by measuring refractive index they stand out among other contaminants. Figure 6 shows THC analysis of a mix of silicone oil and air bubbles. The figure shows data from 2818 particles of which 2616 are identified as silicone oil droplets and 197 of which are identified as air bubbles. As in the previous figures above, silicone oil droplets appear at refractive indexes near 1.41 and are outlined by the orange box in Figure 6a. Since the refractive index of air is 1, air bubbles appear near refractive index of 1 and are outlined by the cyan box in Figure 6a. While the presence of air bubbles is essentially unnoticeable in the particle size distribution of Figure 6b, it is distinct and prominent in the refractive index distribution of Figure 6c. In Figure 6c, the large orange curve represents silicone oil droplets and the smaller, cyan curve towards the bottom of the figure represents air bubbles. Since the refractive indexes of these two species are so different, they are easily and unmistakably distinguishable using xSight.

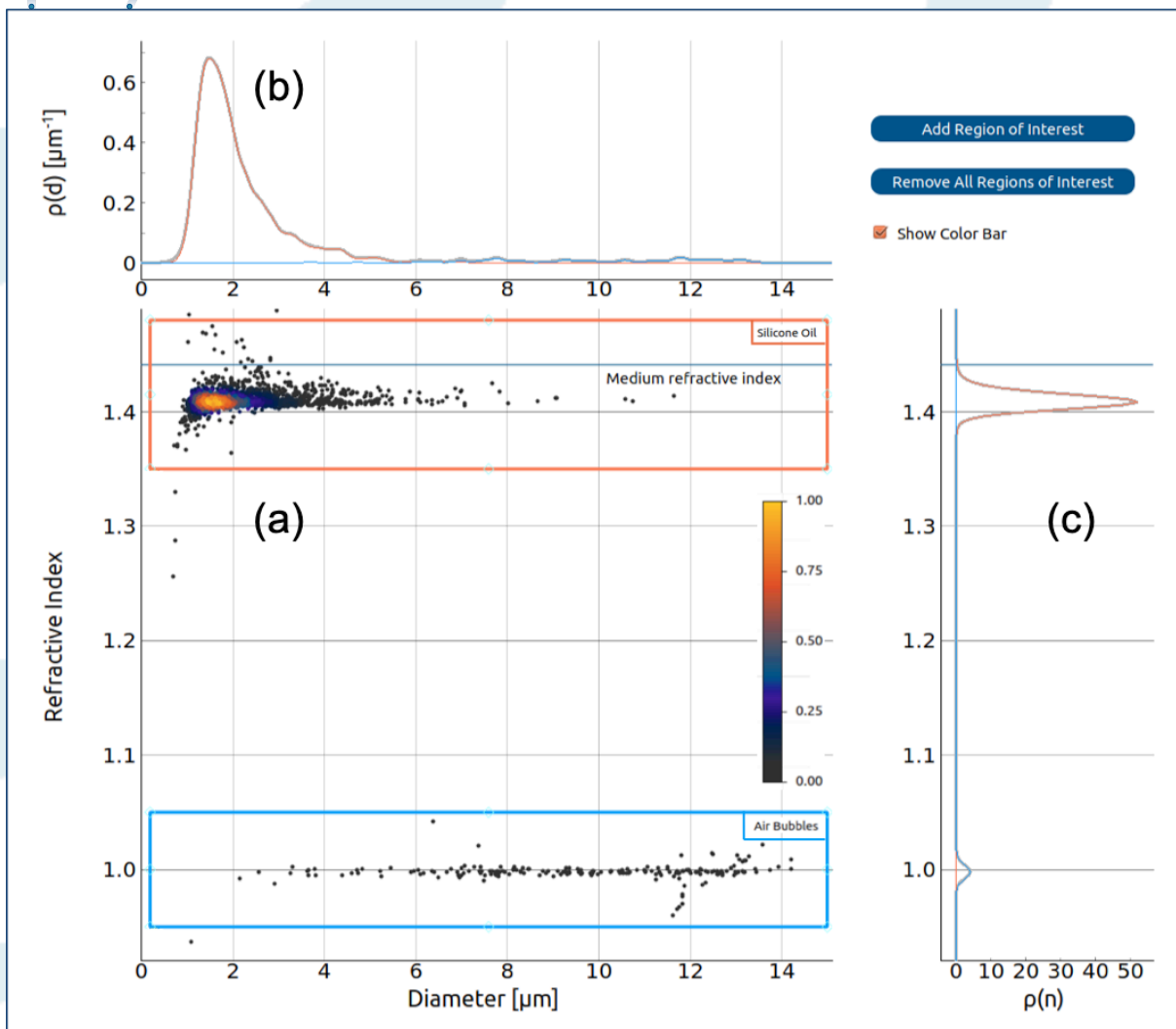


Figure 6: Scatter plot and probability density distributions of a sample of silicone oil and air bubbles.

Using morphology to distinguish and better characterize protein aggregates among other contaminants

In addition to particle size and refractive index, Spheryx provides a novel particle characterization tool: particle morphology. Figure 7 below shows the same sample as Figure 2 (a mix of silicone oil and IgG protein aggregates) but the coloring is based on particle morphology, rather than density of points. In Figure 7a, spherical particles are colored cyan, rod-shaped particles are colored yellow, particles of other shapes are colored orange, and particles with a signal too low for accurate shape determination are colored gray. The violet box in Figure 7a delineates silicone oil droplets in the size range between 800nm and 10μm. Oil droplets in suspension are spherical and the dominant morphology (98%) of the points in the violet box are cyan corresponding to spherical morphology. Particles below 800nm often produce holograms with a signal-to-noise ratio that is too low for accurate morphology identification and most of those particles are labeled as undetermined. In this sample, IgG aggregates, found at refractive indexes between 1.34 and 1.39, show three different morphologies. At sizes from approximately 800nm to 1.5μm and indexes between 1.37 and 1.39, IgG aggregates appear spherical, while most of the aggregates between 1.5μm and 3.5μm appear rod-like, and those larger than 3.5μm have other, more complex shapes. This pattern of morphologies is often present in THC measurements of protein aggregates, but can vary from sample to sample and requires further investigation.

The inset of Figure 7a shows examples of holograms with three different morphologies. The first, on the left, outlined in cyan, is a hologram of a silicone oil droplet with a diameter of $1.32\mu\text{m}$ and a refractive index of 1.407. The hologram's highly symmetric ring pattern is consistent with its spherical assignment. The middle hologram, outlined in yellow, represents an IgG aggregate of a $2.51\mu\text{m}$ diameter and 1.350 refractive index. The interference pattern in this hologram is typical of a rod and is consistent with its rod-like morphology assignment. The hologram on the right, outlined in orange, represents an IgG aggregate of $5.04\mu\text{m}$ diameter and 1.343 refractive index. The interference pattern in this hologram is complex signifying an intricate particle shape and the morphology assignment is appropriately labeled "other shape."

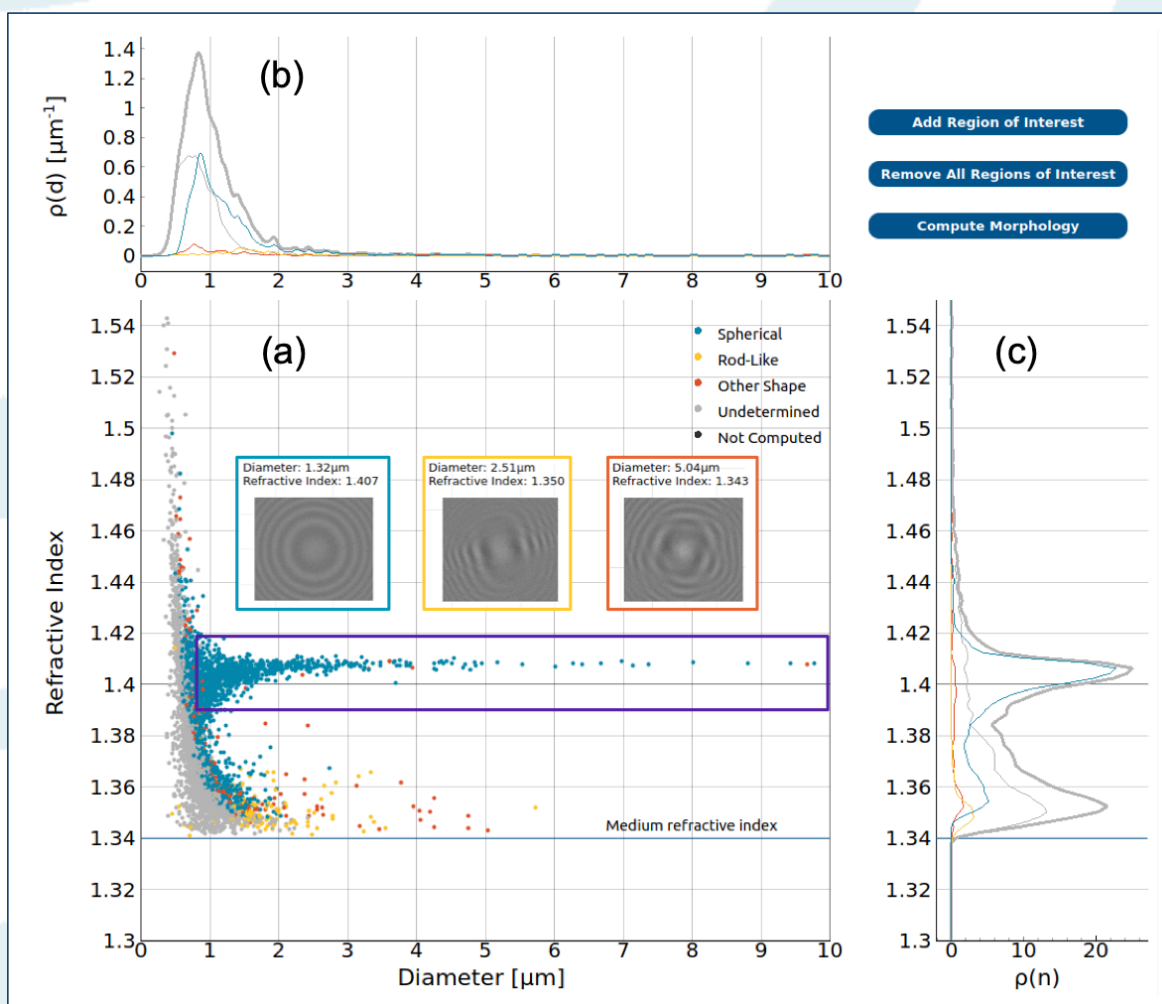


Figure 7: (a) Scatter plot of size vs. refractive index of particles from the same sample as shown in Figure 2. The coloring of points is based on the morphology of the particles they represent: cyan for spherical particles, yellow for rod-like particles, orange for particles of other shapes, light gray for particles with an undetermined shape (usually due to signal being too low for accurate morphology identification). The hologram insets correspond to examples of particles with 3 morphology types. (b) Size density distributions with the same color scheme as in (a) and dark gray curves represent all data. (c) Refractive index density distributions with the same color scheme as in (a) and dark gray curves represent all data.

Figures 7b and 7c show size and refractive index density distributions respectively. The cyan curves represent distributions of spherical particles, the yellow curves represent distributions of rod-shaped particles, the orange curves represent distributions of particles of other shapes, the light gray curves represent particles of undetermined shape, and the dark gray curves are all of the particles in this sample.

While oil droplets and protein aggregates can largely be distinguished by refractive index, some protein particles may appear near refractive index of 1.41 and be confused for oil droplets. Morphology identification can help distinguish the two species.

Figure 8 below shows the morphology characterization of the same sample shown in Figure 4: a mix of oleic acid, silicone oil and IgG aggregates. The two emulsions in this sample, silicone oil and oleic acid, are expected to have spherical particles since droplets in suspension are spherical. The majority of points in those populations, outlined in orange and violet, are cyan corresponding to spherical assignments. As in Figure 7, the IgG aggregate population at refractive indexes below 1.39 shows a mix of three different morphologies: spherical particles, rod-shaped aggregates, and more complex shapes.

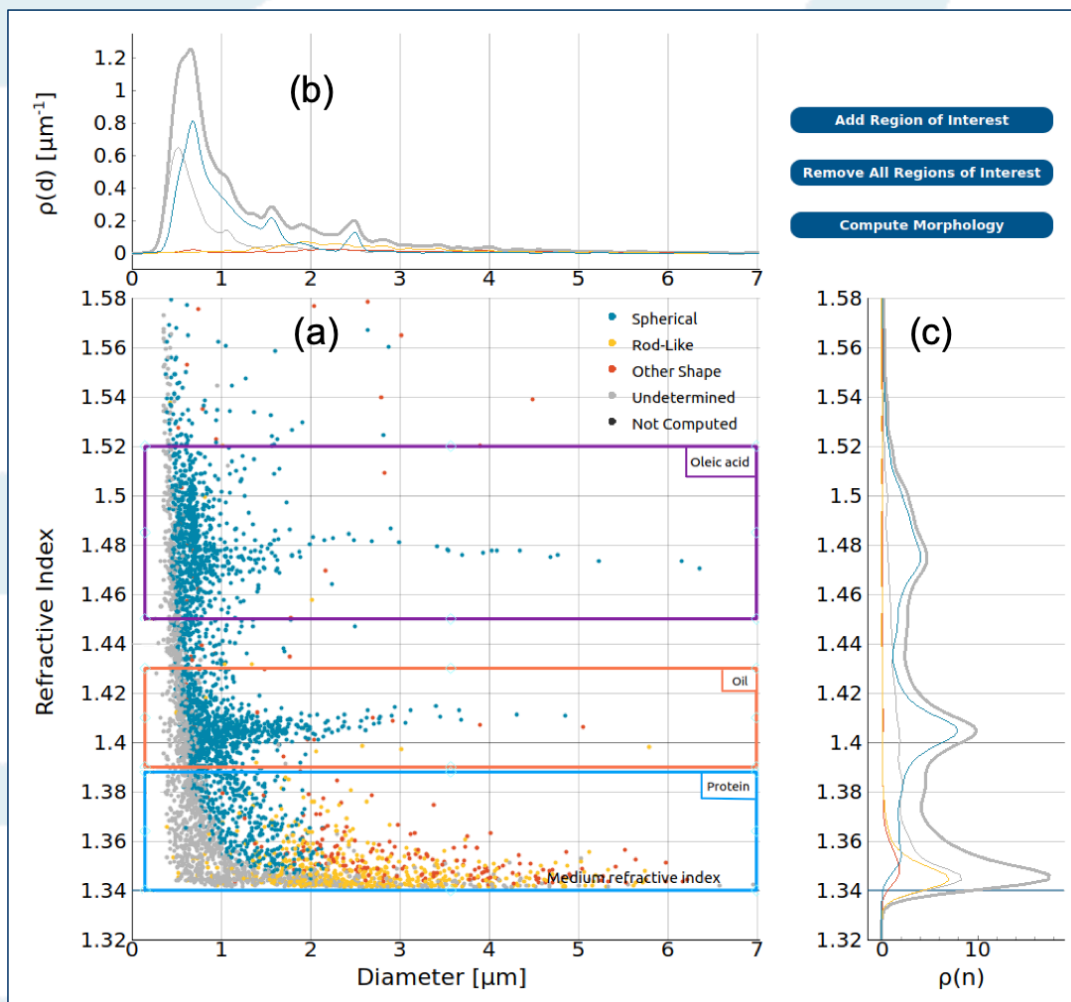


Figure 8: Scatter plot and size and index density distributions as in Figure 7 but for a sample of oleic acid, silicone oil and IgG aggregates.

THC provides robust and reproducible results of protein aggregates and other contaminant

Measurement reproducibility is critically important in the analysis of protein-based formulations. The following size density distribution (Figure 9a) and index density distribution (Figure 9b) show the results of 16 independent xSight measurements of a sample containing IgG aggregates and silicone oil in water. In this sample, the concentration of IgG aggregates is $2.9 \pm 0.3 \times 10^5$ particles/mL, size is 1.25 ± 0.07 μm and refractive index is 1.350 ± 0.001 . The concentration of silicone oil droplets is $6.6 \pm 1.0 \times 10^5$ particles/mL, size is 1.04 ± 0.04 μm , and refractive index is 1.41 ± 0.001 . The curves show excellent reproducibility.

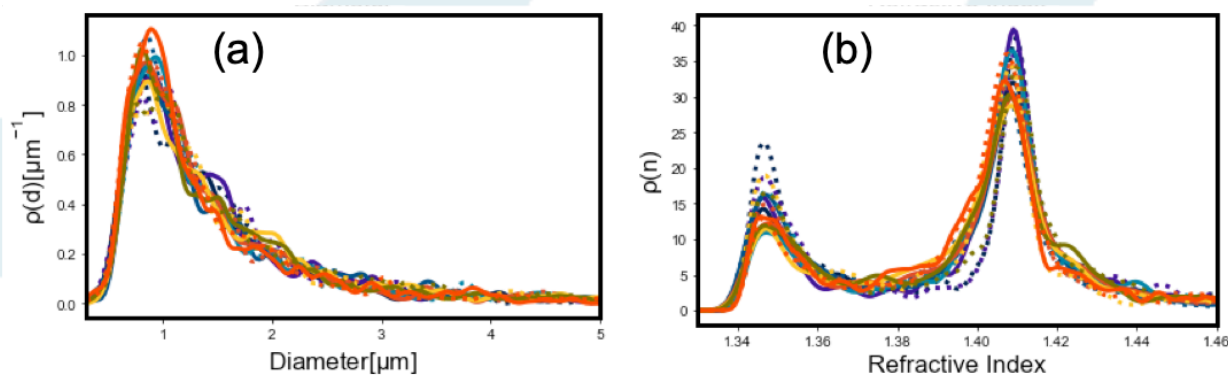


Figure 9: Size and refractive index density distributions of 16 samples consisting of a mix of IgG aggregates and silicone oil droplets. Distributions are plotted on top of each other to demonstrate reproducibility.

Conclusion

THC provides a uniquely informative and quantitative approach to identification and characterization of protein aggregates and other common contaminants in protein formulations. By measuring particle refractive index and morphology in addition to particle size, THC can distinguish numerous species of particles in the same sample even when those species have similar particle sizes. In addition, xSight determines accurate, reproducible concentrations of multiple species in a single measurement. In this note we have demonstrated the ability to quantify and distinguish IgG aggregates mixed with contaminants such as silicone oil, oleic acid, and air bubbles. We have also shown that xSight produces reliable and reproducible results. This approach, using THC, allows users to gain a deeper and more accurate understanding of their samples. Additionally, Spheryx's software provides users with a particle-by-particle characterization as well as statistical overviews of sample properties.

Author:

Dr. Rostislav Boltyanskiy,
Spheryx Senior Scientist II & Director of Scientific Communications

For more information:

info@spheryx.solutions
www.spheryx.solutions

References

- Schellekens H. Bioequivalence and the immunogenicity of biopharmaceuticals. *Nat Rev Drug Discov.* 2002;1:457– 462.
- Wang W. Protein aggregation and its inhibition in bio- pharmaceuticals. *Int J Pharma.* 2005;289:1–30.
- Carpenter JF, Randolph TW, Jiskoot W, Commelin DJA, Middaugh CR, Winter G, et al. Overlooking sub- visible particles in therapeutic protein products: Gaps that may compromise product quality. *J Pharm Sci.* 2009;4:1201– 1205.
- Singh SK, Afonina N, Awwad M, Bechtold-Peters K, Blue JT, Chou D, et al. An industry perspective on the monitoring of subvisible particles as a quality attribute for protein therapeutics. *J Pharm Sci.* 2010;99:3302–3321.
- den Englesman J, Gandel P, Smulders R, Koll H, Smith B, Bassarab S, et al. Strategies for the assessment of



protein aggregates in pharmaceutical biotech product development. *Pharm Res.* 2011;28:920–933.

6. Ratanji KD, Derrick JP, Dearman RJ, Kimber I. Immunogenicity of therapeutic proteins: influence of aggregation. *J. Immunotoxicol.* 2014;11:99-109.
7. Food and Drug Administration. Guidance for Industry: Immunogenicity Assessment for Therapeutic Protein Products. U.S. Department of Health and Human Services; 2014.
8. Panchal J, Kotarek J, Marszal E, Topp EM. Analyzing subvisible particles in protein drug products: a comparison of Dynamic Light Scattering (DLS) and Resonant Mass Measurement (RMM). *AAPS J.* 2014;16(3):440– 451.
9. Hamrang Z, Hussain M, Tingey K, Tracka M, Casas-Finet J, Uddin S, et al. Characterization of stress induced aggregate size distributions and morphological changes of a bi-specific antibody using orthogonal techniques. *J Pharm Sci.* 2015;104(8):2473–2481.
10. Sharma DK, King D, Oma P, Merchant C. Micro-Flow Imaging: Flow microscopy applied to subvisible particulate analysis in protein formulations. *AAPS J.* 2015;12(3):455–464.
11. Zoëlls S, Wiggenghorn M, Winter G, Friess W, Jiskoot W. Flow imaging microscopy for protein particle analysis – A comparative evaluation of four different analytical instruments. *AAPS J.* 2013;15(4):1200–1211.
12. Felsovalyi F, Janvier S, Jouffray S, Soukiassian H, Mangiagalli P. Silicone-oil- based subvisible particles: their detection, interactions, and regulation in prefilled container closure systems for biopharmaceuticals. *J Pharm Sci.* 2012;101:4569-4583.
13. Shah M, Rattray Z, Day K, et al. Evaluation of aggregate and silicone-oil counts in pre-filled siliconized syringes: an orthogonal study characterising the entire subvisible size range. *Int J Pharm.* 2017;519:58-66.
14. Martos A, Koch W, Jiskoot W, et al. Trends on analytical characterization of polysorbates and their degradation products in biopharmaceutical formulations. *J Pharm Sci.* 2017;106:1722-1735.
15. Scherer TM, Leung S, Owyang L, Shire, SJ. Issues and challenges of subvisible and submicron particulate analysis in protein solutions. *AAPS J.* 2012;14:236-243.
16. Wang C, Zhong X, Ruffner DB, et al. Holographic characterization of protein aggregates. *J Pharm Sci.* 2016;105:1074-1085.
17. Kasimbeg PN, Cheong FC, Ruffner DB, Blusewicz JM, Philips LA. Holographic characterization of protein aggregates in the presence of silicone oil and surfactants. *J Pharm Sci.* 2019;108:155-161.
18. Winters A, Cheong FC, Odete MA, et al. Quantitative Differentiation of Protein Aggregates from Other Subvisible Particles in Viscous Mixtures Through Holographic Characterization. *J. Pharm Sci.* 2020; 109:2405-2412.
19. Randolph TW, Schiltz E, Sederstrom D, et al. Do not drop: mechanical shock in vials causes cavitation, protein aggregation, and particle formation. *J Pharm Sci.* 2015;104:602-611.
20. Tobias W, Volkin DB, Mahler HC. Effect of solution properties on the counting and sizing of subvisible particle standards as measured by light obscuration and digital imaging methods. *Eur J Pharm Sci.* 2014;53:95-108.